

Article

Use of Indices in RGB and Random Forest Regression to Measure the Leaf Area Index in Maize

Leonardo Pinto de Magalhães ¹  and Fabrício Rossi ^{2,*} 

¹ Luiz de Queiroz College of Agriculture (ESALQ/USP), Piracicaba 13418-900, Brazil; leonardo.magalhaes@alumni.usp.br

² Faculty of Animal Science and Food Engineering (FZEA/USP), Pirassununga 13635-900, Brazil

* Correspondence: fabricio.rossi@usp.br

Abstract: In the cultivation of maize, the leaf area index (LAI) serves as an important metric to determine the development of the plant. Unmanned aerial vehicles (UAVs) that capture RGB images, along with random forest regression (RFR), can be used to indirectly measure LAI through vegetative indices. Research using these techniques is at an early stage, especially in the context of maize for silage. Therefore, this study aimed to evaluate which vegetative indices have the strongest correlations with maize LAI and to compare two regression methods. RFR, ridge regression (RR), support vector machine (SVM), and multiple linear regression (MLR) regressions were performed in Python for comparison using images obtained in an area cultivated with maize for silage. The results showed that the RGB spectral indices showed saturation when the LAI reached $3 \text{ m}^2 \text{ m}^{-2}$, with the VEG (vegetable index), COM (combination), ExGR (red–green excess), and TGI (triangular greenness index) indices selected for modeling. In terms of regression, RFR showed superior performance with an R^2 value of 0.981 and a root mean square error (RMSE) of $0.138 \text{ m}^2 \text{ m}^{-2}$. Therefore, it can be concluded that RFR using RGB indices is a good way to indirectly obtain the LAI.

Keywords: multiple linear regression; *Zea mays*; remote piloted aircraft; visible spectrum; saturation; remote sensing



Citation: de Magalhães, L.P.; Rossi, F. Use of Indices in RGB and Random Forest Regression to Measure the Leaf Area Index in Maize. *Agronomy* **2024**, *14*, 750. <https://doi.org/10.3390/agronomy14040750>

Academic Editor: Baohua Zhang

Received: 26 January 2024

Revised: 26 February 2024

Accepted: 8 March 2024

Published: 5 April 2024



Copyright: © 2024 by the authors. Licensee MDPI, Basel, Switzerland. This article is an open access article distributed under the terms and conditions of the Creative Commons Attribution (CC BY) license (<https://creativecommons.org/licenses/by/4.0/>).

1. Introduction

The leaf area index (LAI) is an important indicator of plant development related to photosynthesis, energy, and water exchange with the atmosphere [1,2]. It can also be used to indicate crop biomass, in addition to having correlations with canopy microclimate and evapotranspiration characteristics [3]. In addition, monitoring LAI is essential for predicting crop development and determining crop management throughout the growing season [4]. Han et al. [5] observed that an increase in maize plant density leads to an increase in LAI and, consequently, greater light interception. This phenomenon can lead to an increased photosynthetic rate and, consequently, to a higher biomass accumulation by the plant [6], which is a crucial factor for silage production. According to Panigrahi and Das [7], LAI is one of the most important “vegetation characteristics that can be studied using remote sensing spectral reflectance data”.

There are several ways to measure LAI. There are direct and indirect methods, with direct methods measuring leaf area and estimating LAI from harvested leaves or litter. The indirect methods can be based on the relationship with other plant variables or using optical methods [8]. In the literature, several review articles are cited on devices for LAI measurements in the field [9–11]. Several instruments can accomplish this task, such as digital hemispherical photography (DHP) or the LI-COR area meter [8]. A drawback of instruments such as the LI-COR type is that in some cases the leaves must be removed for measurement (destructive method).

Indirect LAI measurement methods using remote sensing have the advantage of being fast and having large spatial coverage. This is in contrast to direct on-site measurements,

which are laborious and time-consuming [12]. Different wavelengths can be related to LAI. Some authors found a high correlation between indices at the red edge wavelength (705 and 750 nm) and LAI compared to other wavelengths [13]. Xue and Su [14] confirm that remote sensing data can be useful for applications in agriculture, among others. Abebe, Tadesse, and Gessesse [15] point out that LAI can be estimated over large areas using remote sensing. In addition, Mulla [16] points out that, depending on the sensor used, the data obtained can be used for crop management as well as for estimating crop productivity. Other types of applications have also been tested, such as microwave remote sensing [17].

Data from RGB sensors can also be used to calculate vegetation and LAI-related indices. These indices have some limitations. Yue et al. [18] observed an underestimation of wheat biomass after canopy closure using RGB data collected by a UAV. The insensitivity of indices in RGB after canopy closure is also reported by Hunt et al. [19].

However, some advantages of indices in RGB can be mentioned. The RGB cameras are cheaper than multispectral cameras and can be used to estimate variables related to the morphological structure of plants [20], although they are less sensitive to plant and leaf structure and thickness [21]. Li et al. [22] highlight that the advantages of RGB cameras over other image acquisition methods include: “ease of use, low cost, a wide range of applications and simple operation”.

According to Rasmussen et al. [23], RGB cameras can quantify crop response similarly to more advanced sensors. The development of unmanned aerial vehicles (UAVs) with RGB cameras has increased work on these systems and their applications due to their high spatial resolution and low cost [24].

The algorithm known as random forest regression (RFR) can be used to relate reflectance data to crop characteristics. Siegmann and Jarmer [25] found that RFR produced better R^2 values than other models for measuring wheat LAI. However, few articles related to LAI and RFR for maize, particularly for silage production. A search conducted on the Web of Science database (as of 23 January 2024) using the terms RGB AND ‘Random Forest Regression’ AND ‘leaf area index’ returned only 16 articles. When the term maize was added, the search results decreased even further (only 5 articles). None of them were carried out in Brazil.

RFR is advantageous over other techniques due to its simplicity [26] and ability to handle small data [27]. This type of regression is cited in the literature for various applications, such as predicting sugarcane productivity [28] and estimating the leaf area index and water content in rice [7]. This technique can be described as an approach that uses the concept of ‘divide and conquer’. It involves initializing fractions of data, developing a decision tree on each of these fractions, and then aggregating the predictions from each tree [29].

Other methods can be used to establish the relationship between reflectance and LAI. Multiple linear regression (MLR) expresses the linear relationship between vegetative indices and LAI, while support vector regression (SVR) establishes a non-linear relationship [30]. To perform regression, an SVM converts sample data that exhibits linear inseparability into a format that shows linear separability and, thus, finds the closest regression plane, including all data in one set [31]. MLR and SVM have their respective disadvantages. MLR requires the operator to select wavelengths, and an inadequate selection can result in worse and mathematically unstable models [32]. On the other hand, SVM does not directly provide probability estimates, and it is necessary to perform an expensive five-fold cross-validation [33]. Kernel methods, such as support vector regression (SVR), typically have few intuitive hyperparameters to tune. They also perform flexible nonlinear input-output mappings. The scatter in the SVR is a direct consequence of the loss function [34]. Alternatively, ridge regression (RR) can efficiently reduce multicollinearity and be applied in productivity and leaf area index (LAI) models [35].

The objective of this study was to indirectly measure the LAI using RFR, considering the importance of obtaining the LAI value more quickly and efficiently, as well as the increasing use of vegetation indices based on RGB. To achieve this goal, the study evaluated

15 different RGB-based indices to determine which one best correlates with maize LAI. Additionally, the study compared different models (RFR versus MLR, RR, and SVM) to measure maize LAI and determine whether RFR performs better.

2. Materials and Methods

2.1. Field Experiments

The research was conducted in Pirassununga, SP, Brazil, at coordinates of 21°59'46" S and 47°25'33" W, and an altitude of 627 m. The study area consisted of a five-hectare section of a maize crop irrigated through a central pivot under the jurisdiction of the USP "Fernando Costa" Campus City Hall (refer to Figure 1). The location was selected for its accessibility in collecting materials, as it is an area of continuous maize cultivation and has sufficient space for conducting flights. The area was divided into 10 plots, each containing a 15-m segment with three rows of 5-m plants. The area was divided into 10 plots, each containing a 15-m segment with three rows of 5-m plants. Samples were collected on five different dates (29 March, 5 April, 12 April, 19 April, and 3 May 2021). The aim was to assess the fresh and dry mass of the plants' aerial parts and determine the leaf area index (LAI).

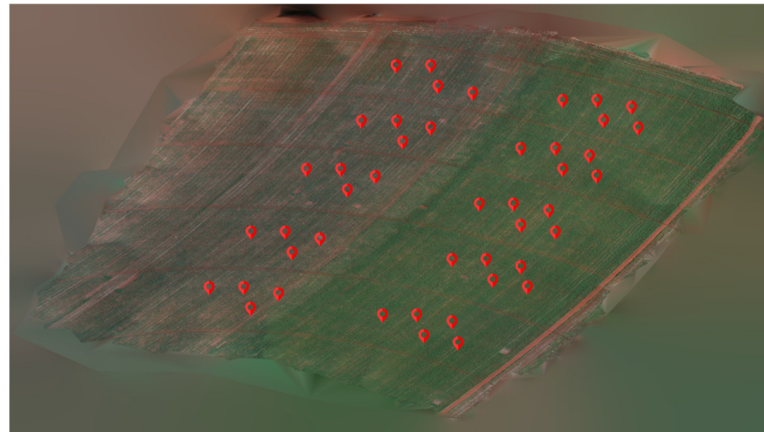


Figure 1. Experimental area cultivated with maize by the Prefecture of the "Fernando Costa" USP Campus (coordinates 21°59'46" S and 47°25'33" W). The image shows the location of the samples taken for the work. 45 samples in total are marked with red dots.

During the evaluation period, aerial images were acquired using Remotely Piloted Aircraft (RPA) (model Phantom 4 Pro, SZ DJI Technology Co., Shenzhen, China) (Figure 2) equipped with a 20 MP camera. The flights were executed at an altitude of approximately 40 m around midday to minimize shading. At this flight altitude, the images had a ground sample distance (GSD) resolution of 1.5 cm. The Pix4D Capture software (Version 4.9.0, Pix4d S.A., Prilly, Switzerland) was used to configure and control the images, with a 70% lateral and frontal overlap. Image data were collected from all plots, except on the final assessment date, when they were gathered from only half of the plots. LAI measurements were conducted on only five plots. The overall dataset consisted of $n = 45$ samples.

The orthophotos were generated using the SfM Agisoft Metashape Professional software (version 1.6.4, Agisoft LLC, Saint Petersburg, Russia) student edition. The processing workflow consisted of image alignment, dense point cloud generation, mesh creation, and orthophoto generation. RGB values for each plot were determined using a developed scripting language. The scripting language can be accessed through this link: https://osf.io/c2prq/?view_only=2aed5df89ba24821a42cd9f21bfa8162 (accessed on 25 January 2024).

The study employed Brevant 2782 maize, which is a simple, early-maturing hybrid with high productivity. The planting density was 70,000 plants per hectare. At each sampling event, the plants were manually extracted and transported to a laboratory where

their fresh weight was measured, and the leaf area index (LAI) was determined using an leaf area integrator (LI-COR Model 3100C, LI-COR, Lincoln, NE, USA). The plants were then dried in an oven at 65 °C for at least 72 h to estimate their dry mass.



Figure 2. Experimental area cultivated with maize and structure for RPA flight.

Vegetation indices were computed using the RGB values extracted from the photographs. These included normalized green (Gn), normalized red (Rn), and normalized blue (Bn), as well as CIVE [36], COM [37], ExG [38], ExGR [39], GLI [40], MPRI (or NGRDI) [41], RGBVI, RGVBI and MGVRI [42], TGI [43], VARI [44], and VEG [45]. The corresponding equations employed for calculating these indices are detailed in Table 1.

Table 1. Equations of the vegetation indices used in the evaluation.

Index	Equation
Bn (Normalized Blue)	$B/(R + G + B)$
Gn (Normalized Green)	$G/(R + G + B)$
Rn (Normalized Red)	$R/(R + G + B)$
CIVE (The index Color Index of Vegetation)	$(0.441 \times Rn) - (0.881 \times Gn) + (0.385 \times Bn) + 18.78745$
COM (Combination)	$(0.25 \times ExG) + (0.3 \times ExGR) + (0.33 \times CIVE) + (0.12 \times VEG)$
ExG (Excess of Green)	$(2 \times gn) - Rn - Bn$
ExGR (Excess of Green and Red)	$ExG - ((1.4 \times Rn) - Gn)$
GLI (Green Leaf Index)	$((2 \times G) - R - B)/((2 \times G) + R + B)$
MGVRI (Modified Green Red Vegetation Index)	$((G \times G) - (R \times R))/((G \times G) + (R \times R))$
MPRI (or NDRI) (Modified Photochemical Reflectance Index)	$G - R/G + R$
RGBVI (Red–Green–Blue Vegetation Index)	$((G \times G) - (R \times B))/((G \times G) + (R \times B))$
RGVBI (Red–Green–Blue Vegetation Index)	$(G - (B \times R))/((G \times G) + (B \times R))$
TGI (Triangular Greenness Index)	$G - (0.39 \times R) - (0.61 \times B)$
VARI (Visible Atmospherically Resistant Index)	$(G - R)/((G + R) - B)$
VEG (Vegetative Index)	$Gn/((Rn \times 0.667) \times (Bn^{0.333}))$

Table 2 summarizes the phenological stage during which the plants were analyzed, images were obtained, and leaves were collected for area measurement. The analyses began at V6 and extended until VT (flowering).

Table 2. Phenological stage of maize during the experiment.

Date	Phenological Stage
29 March 2021	V6
5 April 2021	V8
12 April 2021	V9
19 April 2021	V10
3 May 2021	VT

2.2. Statistical Analysis

The leaf area index (LAI) was used to select indices with the highest correlation, using Pearson's correlation test. This test measures the relationship between two continuous variables and assigns a value between -1 and 1 , where 0 indicates no correlation, 1 indicates total positive correlation, and -1 indicates total negative correlation (Equation (1)). Individual simple regressions were calculated using the indices and the LAI values to evaluate the quality of the LAI calculation. The determination coefficient (R^2) of the regressions was compared with values obtained via random forest regression (RFR) and multiple linear regression (MLR).

$$r_{xy} = \frac{\sum_{i=1}^n (x_i - \bar{x})(y_i - \bar{y})}{\sqrt{(\sum_{i=1}^n (x_i - \bar{x})^2) \sqrt{(\sum_{i=1}^n (y_i - \bar{y})^2)}} \quad (1)$$

where, n = sample size, x_i and y_i are the individual sample points, and \bar{x} and \bar{y} are the mean values of x and y .

The process of selecting indices for the LAI measurement model was carried out using the 'ols_step_both_aic' function in the R statistical program (RStudio, version 4.2.2, Boston, MA, USA). This function uses the Akaike information criteria (AIC) to guide variable selection for the model. The AIC criterion favors models with fewer variables, based on the principle of simplicity. A lower AIC value indicates a more precise definition of the model by the selected variables.

The Akaike information criterion (AIC) is a quality estimator for statistical models concerning a given dataset. It estimates the prediction error of each model. The AIC quantifies the amount of information lost through the modeling process.

This method is named after its originator, the Japanese statistician Hirotugu Akaike. The model to be adopted is determined by the AIC, which is calculated using the following equation based on its quality and simplicity.

$$AIC = 2k - 2\ln(\hat{L}) \quad (2)$$

where k is the number of estimated parameters in the model and is the maximized value of the likelihood function for the model.

The multiple linear regression (MLR) technique utilized the ordinary least squares (OLS) method in R script to estimate unknown parameters in a linear regression model. The random forest regression (RFR), ridge regression (RR), and support vector machine (SVM) analyses employed the sklearn library in Python. Results were analyzed and graphs were produced using a Python script.

The RFR is a meta-estimator that fits a set of classification decision trees on various subsamples of the total data and employs averaging to enhance predictive accuracy. It constitutes an ensemble of diverse predictor trees, or a forest, wherein each tree is generated from a random vector independently sampled with the same distribution for each tree.

In the sklearn.ensemble.RandomForestRegressor, a function of Python, the parameters governing the regression process include n_estimators (number of trees in the forest), criterion (function to measure the quality of a split), min_samples_split (minimum number

of samples required to split an internal node), `min_samples_leaf` (minimum number of samples required to be in a leaf node), among others. The specified parameter values for the analysis were: `n_estimators = 100`, `criterion = mean squared error`, `min_samples_split = 2`, and `min_samples_leaf = 1`.

Ordinary least squares (OLS) linear regression is a statistical technique used to model linear relationships between an objective variable and one or more predictor variables. To calculate the line that best fits the data, the R script uses the `lm()` function, which will obtain the slope and intercept coefficients.

The model analysis computed three metrics: R-squared (R^2) (Equation (3)), mean absolute error (MAE) (Equation (4)), and root mean squared error (RMSE) (Equation (5)). These values were generated by the Python algorithm. Graphs were also plotted to depict the calculated LAI values versus the observed LAI values.

$$R^2 = 1 - \frac{\sum(\hat{y}_i - y_i)}{\sum(y_i - \bar{y})} \quad (3)$$

where \hat{y}_i = prediction, y_i = actual value of LAI, and \bar{y} = mean value.

$$MAE = \frac{|y - \hat{y}|}{n} \quad (4)$$

where \hat{y} = prediction, y = actual value of LAI, and n = number of samples.

$$RMSE = \sqrt{\left(n^{-1} \sum_{i=1}^n (y_i - y_{o_i})^2\right)} \quad (5)$$

where n = number of samples, y_i = LAI predicted, and y_{o_i} = LAI observed.

To enhance comprehension of the study and its progression, Figure 3 provides a summary of the steps and analyses conducted.

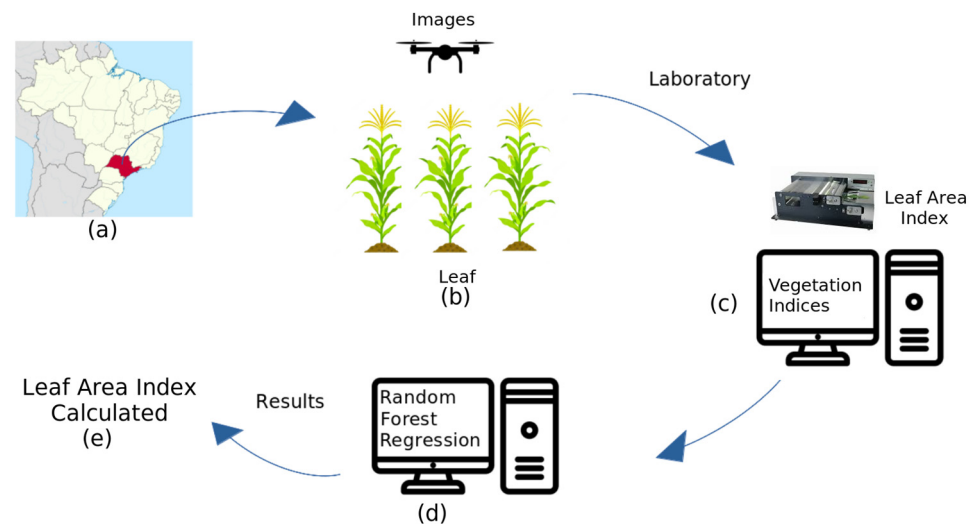


Figure 3. This is a flowchart outlining the steps and analyses conducted during the research. The location (State) in Brazil where the research was carried out is labeled as (a), while (b) represents the area where the images and plant samples were obtained on the same dates. The samples were taken to the laboratory to obtain the leaf area and calculate the indices using the images, as shown in (c). The simulation was carried out in the Python language using the data obtained in (c), as indicated in (d). Finally, the LAI calculation value was obtained for the models in step (e).

3. Results

Regarding Pearson's correlation coefficient, all indices showed values above 0.8 (Figure 4) when considering the complete dataset across all assessment dates. The only exception to this trend was observed in the case of normalized blue (Bn), which displayed a

correlation coefficient of 0.19, indicating a weak correlation (less than 0.5). The correlation coefficient of normalized red (Rn) displayed a negative value, which is attributed to the absorption occurring in chlorophylls a and b within the red wavelength [46]. As the leaf area of plants increased, the quantity of absorbing chlorophyll in this wavelength also increased, leading to a reduction in reflectance. This explains the negative correlation.

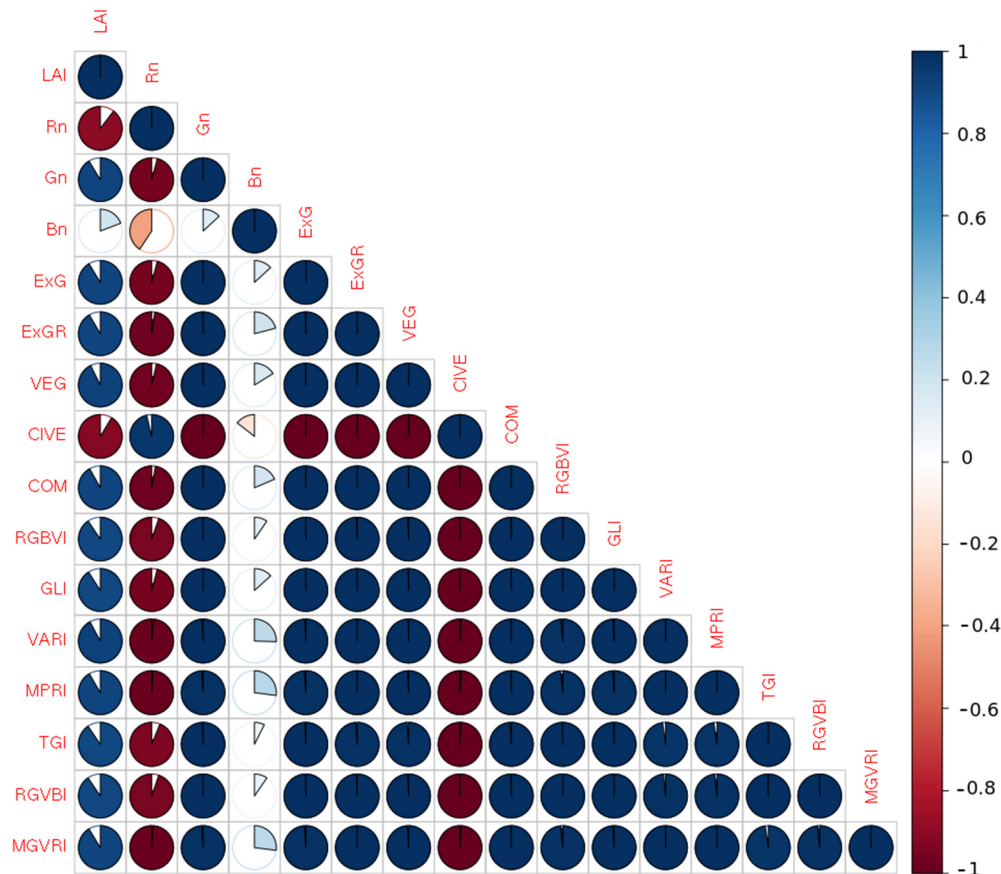


Figure 4. Pearson correlation between LAI and vegetation indices in RGB on all analysis dates. LAI = Leaf Area Index, Bn = Normalized Blue, Gn = Normalized Green, Rn = Normalized Red, CIVE = The index Color Index of Vegetation, COM = Combination, ExG = Excess of Green, ExGR = Excess of Green and Red, GLI = Green Leaf Index, MGVRI = Modified Green Red Vegetation Index, MPRI= Modified Photochemical Reflectance Index, RGBVI = Red–Green–Blue Vegetation Index, RGVBI = Red–Green–Blue Vegetation Index, TGI = Triangular Greenness Index, VARI = Visible Atmospherically Resistant Index, VEG = Vegetative Index.

A negative correlation was found between the CIVE index (Equation (4)—Table 1) and the leaf area index (LAI). This correlation is due to the negative coefficient in Equation (4), which pertains to the green reflectance band. As the LAI increases, a greater proportion of green becomes a component of the captured image’s color composition.

Most RGB indices became insensitive after the LAI reached 2. During the final phase of the analysis, the TGI showed a stronger correlation with the field-measured LAI. As the plant approached the reproductive stage, all indices showed a decrease in the Pearson correlation coefficient value.

For model development, we selected VEG, COM, ExGR, and TGI indices (Model 4). This combination resulted in the lowest AIC value (36.773) compared to other configurations with different indices (Table 3). Adding more indices to the model (starting from model 5 in Table 3) did not reduce the AIC value. On the contrary, the AIC value increases, indicating that the error of these models is greater. As more indices are added, the models become less simple.

Table 3. Subset regression summary.

Model Index	Predictors
1	VEG
2	MGVRI VARI
3	MGVRI MPRI TGI
4	ExGR COM TGI VEG
5	ExGR COM Rn TGI VEG
6	ExGR COM MGVRI TGI VARI VEG
7	ExGR COM MGVRI Rn TGI VARI VEG
8	ExGR COM MGVRI MPRI Rn TGI VARI VEG

The ExGR and COM indices are composed of different combinations of indices. ExGR uses the values of the normalized green and red indices, while COM uses the values of ExGR, ExG, CIVE, and VEG. Thus, the two indices contribute additional information to the LAI measurement model, resulting in more accurate models.

The RFR model showed a high R-squared (R^2) value of 0.98, while the MLR, SVM, and RR models achieved values of 0.89, 0.90, and 0.86, respectively. In addition, the RFR model also resulted in lower values for both root mean squared error ($0.14 \text{ m}^2 \text{ m}^{-2}$, compared to 0.34 for MLR, 0.37 for RR, and 0.32 for SVM) and absolute error ($0.08 \text{ m}^2 \text{ m}^{-2}$, compared to 0.25 for MLR, 0.27 for RR, and 0.23 for SVM). Table 4 summarizes the data for each model. The improvement in the R^2 value and the reduction in error through the use of the RFR model are evident. An increase in the R^2 value indicates that the predicted values from this model have a better fit than those obtained from other models.

Table 4. Results of LAI prediction with multiple linear regression (MLR), random forest regression (RFR), ridge regression (RR), and support vector machine (SVM).

	R^2	MAE ($\text{m}^2 \text{ m}^{-2}$)	RMSE ($\text{m}^2 \text{ m}^{-2}$)
MLR	0.89	0.25	0.34
RFR	0.98	0.08	0.14
RR	0.86	0.27	0.37
SVM	0.90	0.23	0.32

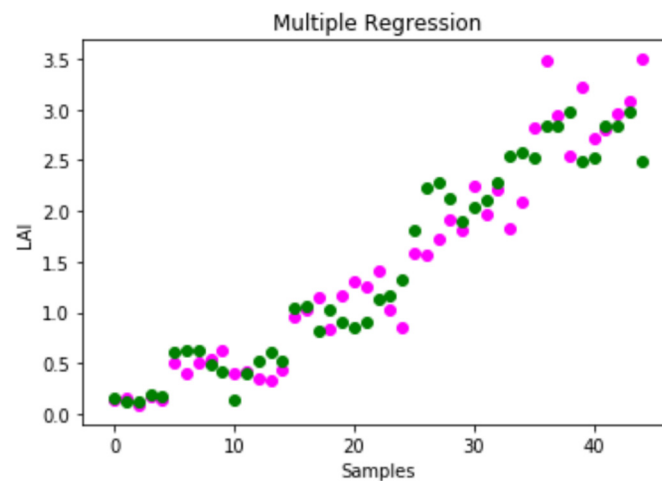
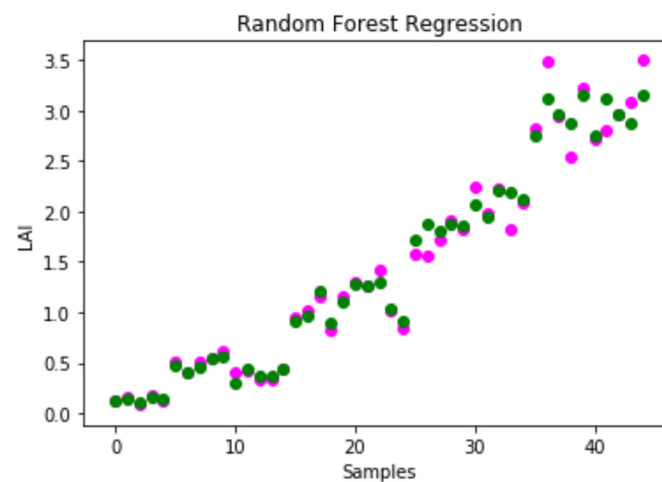
For comparison purposes, we developed calculation models of the leaf area index (LAI) using each of the selected indices individually. The results are shown in Table 5. In a linear regression analysis, the VEG index showed superior performance, with a higher coefficient of determination (R^2) and a lower root mean square error (RMSE). It is important to note that the triangular greenness index (TGI) displayed poorer performance in predicting LAI despite reaching saturation at a later stage than the other indices. The models using the composite index (COM), excess green index (ExGR), and TGI followed (Table 5).

Table 5 shows that using only one index in each model results in a lower R^2 value and a consequent increase in RMSE. A higher RMSE value indicates lower precision in measuring the LAI, leading to an error increase of almost 0.5 m^2 .

Figures 5 and 6 depict the models derived through RFR and MLR, respectively, revealing that the measurement error increases after the thirtieth observation. The disparity between the model-derived and field-measured values grew from the 30th sample onward due to index saturation. As previously discussed, all indices experienced saturation at LAI values exceeding 3, causing them to lose sensitivity to LAI variation. Even with an increase in LAI, the vegetative index does not increase with the same intensity. However, the TGI has lower saturation, which mitigates this issue in the models.

Table 5. Results of LAI prediction with the single vegetation index.

	R ²	RMSE (m ² m ⁻²)
VEG	0.86	0.39
COM	0.84	0.41
ExGR	0.84	0.41
TGI	0.82	0.44

**Figure 5.** Relationship between the observed (pink) and calculated (green) values by the LAI model for multiple linear regression.**Figure 6.** Relationship between the observed (pink) and calculated (green) values by the LAI model for random forest regression.

This phenomenon increases measurement error as saturation intensifies. However, the RFR-derived model reduces this effect, increasing the R-squared value and decreasing the mean error. Even the MLR-based model maintains an R-squared value higher than that of the LAI calculated using a single index alone.

Figure 6 demonstrates the relationship between the LAI values calculated using the RFR and those observed in the field. It is observed that the points are close to the 1:1 line, demonstrating a good relationship between the real value and the simulated one. This proximity changes in the latest observations. This fact occurs, as already discussed, because of the saturation of indices.

As will be further discussed in the next section, RFR has the advantage of reducing LAI measurement error to a greater extent. This factor is represented in Figure 7, and the

result presented in this figure also demonstrates that even using RGB indices, the model's efficiency level is high.

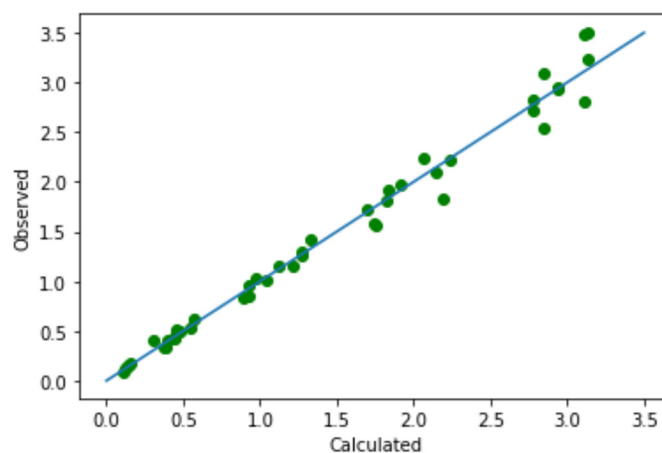


Figure 7. Values of the calculated and observed of LAI model for random forest regression. The blue line is the regression line and the green dots are the dispersion points of the calculated versus observed LAI (Leaf Area Index).

4. Discussion

When examining the comprehensive dataset across all assessment dates, the indices that showed the highest correlation coefficients were VEG (0.927) and VARI (0.921). Shao et al. [47] found a Pearson correlation coefficient of 0.7 between the leaf area index and the VARI in maize. In a study by Qiao et al. [48], different correlation coefficients were observed between the LAI and the VARI index at different maize development stages. During the initial developmental phase, the authors found a correlation coefficient of 0.37. The correlation coefficient increased to 0.83 in the stages before flowering. At the VT stage (tanning), it was 0.63, whereas in stages R1, R2, and R3, the coefficients were 0.38, 0.12, and 0.38, respectively. This variability in the correlation between the LAI and the VARI index across different growth stages highlights the fluctuating nature of their relationship.

In the current study, we observed a similar pattern where correlation coefficient values varied when the data were segmented into distinct periods. During the growth stages V7 to V9, before the LAI surpassed $1 \text{ m}^2 \text{ m}^{-2}$ ($n = 15$), we found that the following indices exhibited correlation coefficients exceeding 0.7: Rn (with a negative correlation), ExGR, VEG, COM, VARI, MPRI, and MGARI. During the interval from LAI = 1 to LAI = 2, which spans stages V9 to V10, the following indices exhibited correlation coefficients above 0.6: Rn, VARI, MPRI, TGI, and MGARI.

Toward the end of the analysis, when the LAI exceeded $2 \text{ m}^2 \text{ m}^{-2}$, and even reached values exceeding 3, the indices showed significantly lower correlations. The only index that surpassed 0.5 was the triangular greenness index (TGI). In the final analysis period, the remaining indices displayed correlation coefficients ranging between 0.4 and 0.47, with Rn exhibiting an even lower coefficient of -0.383 .

The above findings emphasize the importance of selecting appropriate indices based on the crop development stage. During the early stages of plant growth, there is higher reflectance in the red spectrum. However, as biomass accumulates, this value decreases [49]. Therefore, indices that strongly correlate with this type of red reflectance, such as normalized red (Rn) or ExGR, may be more suitable for use during the initial crop development stages. As the canopy becomes denser, indices that are more strongly associated with green reflectance, such as VARI and MPRI, show a stronger correlation with the leaf area index (LAI). After the canopy has closed and the maximum LAI value has been reached, the TGI index becomes the more appropriate choice, as indicated by the analyzed data.

The TGI index was originally designed to correlate with the chlorophyll content of plants at the canopy level. It exhibits the highest correlation when the LAI exceeds

$2 \text{ m}^{-2} \cdot \text{m}^{-2}$. According to Hunt et al. [43], this index experiences rapid growth with LAI values ranging from 1 to 2, eventually saturating beyond this threshold. The researchers emphasized that the TGI index's reduced responsiveness with LAI values surpassing 2 is due to the closure of the canopy, rather than the LAI value per se. In a separate study, Hunt et al. [19] noted that the NGRDI index (referred to here as MPRI) likewise saturates as LAI values exceed 2. Zhang et al. [50] also observed a slightly greater than 3 LAI value within this timeframe, with a plant density of $67,500 \text{ plants ha}^{-1}$. Consequently, during this stage, the plant's LAI stabilizes, followed by a subsequent decline leading up to the R3 stage.

This index is also highly sensitive to variations in chlorophyll content. Between stages VT and R4, although there is a decrease in LAI, there is an increase in chlorophyll levels [51]. Therefore, the stronger correlation observed for the TGI during the last third of the data analysis can be explained by this aspect. As a result, the TGI index has the potential to detect fluctuations in chlorophyll content more precisely, which coincides with the LAI stabilization post-VT.

Different RGB indices have been used in literature to calculate LAI. In a study on winter wheat, Hasan et al. [52] used a quadratic model with the VARI index, resulting in an R^2 of 0.726. Additionally, Ballesteros et al. [53] achieved an R^2 of 0.754 by using a linear model with the VARI index. Marcial-Pablo [54] determined that the NDRI index exhibited the most favorable outcomes during the senescence growth stages of maize when examining vegetation coverage fraction from RGB data. Sanches et al. [55] identified correlations of 0.49 and 0.59 between LAI and the NDRI index in sugarcane across two assessment dates. Chen et al. [56] observed a strong correlation between the VARI index and leaf water content, which may explain its relationship with leaf growth. However, Gholinejad and Fatemi [57] found that the GLI and MPRI (NGRDI) indices were not very accurate in assessing changes in vegetation over time. The study's findings revealed higher values than those reported in the literature when using the indices separately or in combination through modeling with MLR, RR, SVM, and RFR.

Our models utilize the VEG, ExGR, COM, and TGI indices to measure the evolution of LAI by adding different spectral information. VEG shows a better correlation with LAI during the intermediate stages of plant development due to the preponderance of green in its calculation. In contrast, ExGR, which has a greater weight of reflectance in red, shows a greater correlation in the initial stages when the soil is more exposed. The selected indices (COM and ExGR) aggregate information from other indices due to their configuration. To calculate COM, the values of ExG, ExGR, VEG, and CIVE indices are required. Therefore, this index provides additional information about the reflectance variation, resulting in a better representation of the LAI variation. The TGI index showed saturation later than the other indexes concerning the LAI. This factor reduces data dispersion after the saturation of other indices and minimizes errors.

The models obtained through RFR, MLR, RR, and SVM present superior results compared to calculating LAI using just one index. The MLR-derived model showed an R^2 value of 0.8911, while RFR showed an R^2 value of 0.9819. These results, coupled with the lower mean error, indicate that the obtained models are more accurate in determining the LAI value in maize. The model incorporating the four indices derived through RFR is the most suitable for assessing the development of this aspect within the crop.

Panigrahi and Das [7] achieved an RMSE value of $0.85 \text{ m}^2 \text{ m}^{-2}$ for wheat LAI using RFR and multispectral images. In contrast, we obtained a lower RMSE value (0.08) for wheat LAI using RGB images, which are more cost-effective and easier to use [22]. For white wheat, Siegmann and Jarmer [25] reported RMSE values of 0.337 and $0.476 \text{ m}^2 \text{ m}^{-2}$ for the years 2011 and 2012, respectively. In a study by Liu et al. [58], the root mean square error (RMSE) for predicting the LAI of maize using RFR and SVM with RGB images was approximately $0.67 \text{ m}^2 \text{ m}^{-2}$ and 0.65, respectively, which is higher than the value found in our work. Du et al. [24] also used RFR and RGB images and observed an RMSE of $0.21 \text{ m}^2 \text{ m}^{-2}$. Luo et al. [30] measured LAI with SVM and hyperspectral data and observed an RMSE of 0.634, which is higher than our observed value for SVM with RGB images.

Chai and Draxler [59] argue that using root mean square error (RMSE) provides a comprehensive picture of the error distribution. Therefore, it indicates how the error is distributed across all samples. The RMSE obtained in our model demonstrates that the values align closely with those reported in the literature, even falling below those presented in other articles. Furthermore, our model used only 4 parameters, while other models discussed used up to 16 parameters.

According to Wolff et al. [60], the selection of devices depends on the mapping objective. Our results demonstrate that using RGB indices, combined with modeling via RFR, yields superior results compared to works with multispectral images. RGB cameras can deliver similar or better results than multispectral cameras in monitoring the evolution of plant development [61], at a lower financial and computational cost. Additionally, our study evaluates indices such as COM, VEG, and TGI, which are infrequently mentioned in the literature for measuring LAI. These analyses enhance our understanding of the relationship between these indices and LAI, furthering the discussion about the point at which they become saturated and indicating avenues for future research on the use of indices in conjunction with RGB and RFR for measuring LAI.

Further research should be conducted to validate the models in different maize planting arrangements. Additionally, other spectral indices or datasets could be compared with the obtained results for a more comprehensive discussion and validation of the models described in this paper.

5. Conclusions

The study analyzed data that showed RFR with RGB indices as a viable option for LAI prediction models in maize. However, these indices showed saturation when the LAI was around $3 \text{ m}^2 \text{ m}^{-2}$. The correlation of the indices with the LAI indicated that indices with greater sensitivity to fluctuations in red reflectance, such as Rn and ExGR, had a stronger correlation in the initial stages of crop development. During the phases from emergence (VE) to V6, when vegetation cover is minimal, most of the reflectance captured by the sensors comes from the soil. As the plant grows and produces more leaves, the amount of red reflectance decreases. This is because the soil contributes less, and the chlorophylls a and b absorb more red light. Therefore, it is more appropriate to use green-responsive indices until the plant blooms.

The regression model was prepared using the ExGR, COM, TGI, and VEG indices out of the 15 analyzed. The use of RFR with these indices reduced the error between the calculated and observed LAI values. Additionally, the R^2 value of this model exceeded that of both the single index models and the models based on MLR, RR, or VSM. The data show that both indices and models selected through RFR can measure LAI and assess maize development over time. The results suggest that the RFR model outperforms the others analyzed and those found in the literature.

Author Contributions: Conceptualization, L.P.d.M. and F.R.; methodology, L.P.d.M. and F.R.; software, L.P.d.M.; validation, L.P.d.M.; formal analysis, L.P.d.M. and F.R.; investigation, L.P.d.M.; resources, F.R.; data curation, L.P.d.M.; writing—original draft preparation, L.P.d.M.; writing—review and editing, L.P.d.M.; visualization, L.P.d.M.; supervision, F.R.; project administration, F.R.; funding acquisition, F.R. All authors have read and agreed to the published version of the manuscript.

Funding: This study was financed in part by the Coordenação de Aperfeiçoamento de Pessoal de Nível Superior—Brasil (CAPES)—Finance Code 001.

Data Availability Statement: Publicly available datasets were analyzed in this study. The data will be found here: https://osf.io/c2prq/?view_only=2aed5df89ba24821a42cd9f21bfa8162 (accessed on 25 January 2024).

Conflicts of Interest: The authors declare no conflict of interest.

References

1. Gitelson, A.A.; Viña, A.; Arkebauer, T.J.; Rundquist, D.C.; Keydan, G.; Leavitt, B. Remote Estimation of Leaf Area Index and Green Leaf Biomass in Maize Canopies. *Geophys. Res. Lett.* **2003**, *30*, 1248. [[CrossRef](#)]
2. Bian, M.; Chen, Z.; Fan, Y.; Ma, Y.; Liu, Y.; Chen, R.; Feng, H. Integrating Spectral, Textural, and Morphological Data for Potato LAI Estimation from UAV Images. *Agronomy* **2023**, *13*, 3070. [[CrossRef](#)]
3. Rasti, S.; Bleakley, C.J.; Holden, N.M.; Whetton, R.; Langton, D.; O'Hare, G. A Survey of High Resolution Image Processing Techniques for Cereal Crop Growth Monitoring. *Inf. Process. Agric.* **2021**, *9*, 300–315. [[CrossRef](#)]
4. Wang, Y.; Zhou, H.; Ma, X.; Liu, H. Combining Data Assimilation with Machine Learning to Predict the Regional Daily Leaf Area Index of Summer Maize (*Zea mays* L.). *Agronomy* **2023**, *13*, 2688. [[CrossRef](#)]
5. Han, K.; Liu, B.; Liu, P.; Wang, Z. The Optimal Plant Density of Maize for Dairy Cow Forage Production. *Agron. J.* **2020**, *112*, 1849–1861. [[CrossRef](#)]
6. Jia, Q.; Sun, L.; Mou, H.; Ali, S.; Liu, D.; Zhang, Y.; Zhang, P.; Ren, X.; Jia, Z. Effects of Planting Patterns and Sowing Densities on Grain-Filling, Radiation Use Efficiency and Yield of Maize (*Zea mays* L.) in Semi-Arid Regions. *Agric. Water Manag.* **2017**, *201*, 287–298. [[CrossRef](#)]
7. Panigrahi, N.; Das, B.S. Evaluation of Regression Algorithms for Estimating Leaf Area Index and Canopy Water Content from Water Stressed Rice Canopy Reflectance. *Inf. Process. Agric.* **2021**, *8*, 284–298. [[CrossRef](#)]
8. Fang, H.; Baret, F.; Plummer, S.; Schaepman-Strub, G. An Overview of Global Leaf Area Index (LAI): Methods, Products, Validation, and Applications. *Rev. Geophys.* **2019**, *57*, 739–799. [[CrossRef](#)]
9. Bréda, N. Ground-based Measurements of Leaf Area Index: A Review of Methods, Instruments and Current Controversies. *J. Exp. Bot.* **2003**, *54*, 2403–2417. [[CrossRef](#)]
10. Jonckheere, I.; Fleck, S.; Nackaerts, K.; Muys, B.; Coppin, P.; Weiss, M.; Baret, F. Review of Methods for in Situ Leaf Area Index Determination Part I. Theories, Sensors and Hemispherical Photography. *Agric. For. Meteorol.* **2004**, *121*, 19–35. [[CrossRef](#)]
11. Weiss, M.; Baret, F.; Smith, G.; Jonckheere, I.; Coppin, P. Review of Methods for in Situ Leaf Area Index (LAI) Determination: Part II. Estimation of LAI, Errors and Sampling. *Agric. For. Meteorol.* **2004**, *121*, 37–53. [[CrossRef](#)]
12. Zheng, G.; Moskal, L.M. Retrieving Leaf Area Index (LAI) Using Remote Sensing: Theories, Methods and Sensors. *Sensors* **2009**, *9*, 2719. [[CrossRef](#)] [[PubMed](#)]
13. Verma, B.R.; Thakore, T.; Prasad, R.; Srivastava, P.K.; Yadav, S.A.; Singh, P.; Singh, R. Investigation of Optimal Vegetation Indices for Retrieval of Leaf Chlorophyll and Leaf Area Index Using Enhanced Learning Algorithms. *Comput. Electron. Agric.* **2022**, *192*, 106581. [[CrossRef](#)]
14. Xue, J.; Su, B. Significant Remote Sensing Vegetation Indices: A Review of Developments and Applications. *J. Sens.* **2017**, *2017*, 1353691. [[CrossRef](#)]
15. Abebe, G.; Tadesse, T.; Gessesse, B. Estimating Leaf Area Index and Biomass of Sugarcane Based on Gaussian Process Regression Using Landsat 8 and Sentinel 1A Observations. *Int. J. Image Data Fusion* **2022**, *14*, 58–88. [[CrossRef](#)]
16. Mulla, D.J. Twenty Five Years of Remote Sensing in Precision Agriculture: Key Advances and Remaining Knowledge Gaps. *Biosyst. Eng.* **2013**, *114*, 358–371. [[CrossRef](#)]
17. Yadav, S.A.; Prasad, R.; Yadav, V.P.; Verma, B.; Singh, S.; Sharma, J.; Srivastava, B.K. Far-field Bistatic Scattering Simulation for Rice Crop Biophysical Parameters Retrieval Using Modified Radiative Transfer Model at X- and C-band. *Remote Sens. Environ.* **2022**, *272*, 112959. [[CrossRef](#)]
18. Yue, J.; Yang, G.; Tian, Q.; Feng, H.; Xu, K.; Zhou, C. Estimate of Winter-Wheat Above-Ground Biomass Based on UAV Ultrahigh-Ground-Resolution Image Textures and Vegetation Indices. *ISPRS J. Photogramm. Remote Sens.* **2019**, *150*, 226–244. [[CrossRef](#)]
19. Hunt, E.R.; Cavigelli, M.A.; Daughtry, C.S.; McMurtrey, J.E.; Walthall, C.L. Evaluation of Digital Photography from Model Aircraft for Remote Sensing of Crop Biomass and Nitrogen Status. *Precis. Agric.* **2005**, *6*, 359–378. [[CrossRef](#)]
20. Jin, X.; Zarco-Tejada, P.J.; Schmidhalter, U.; Reynolds, M.P.; Hawkesford, M.J.; Varshney, R.K.; Yang, T.; Nie, C.; Li, Z.; Ming, B.; et al. High-Throughput Estimation of Crop Traits: A Review of Ground and Aerial Phenotyping Platforms. *IEEE Geosci. Remote Sens. Mag.* **2021**, *9*, 200–231. [[CrossRef](#)]
21. Prey, L.; von Bloh, M.; Schmidhalter, U. Evaluating RGB Imaging and Multispectral Active and Hyperspectral Passive Sensing for Assessing Early Plant Vigor in Winter Wheat. *Sensors* **2018**, *18*, 2931. [[CrossRef](#)]
22. Li, X.; Xu, X.; Xiang, S.; He, S.; Wang, W.; Xu, M.; Liu, C.; Yu, L.; Liu, W.; Yang, W. Soybean Leaf Estimation Based on RGB Images and Machine Learning Methods. *Plant Methods* **2023**, *19*, 59. [[CrossRef](#)]
23. Rasmussen, J.J.; Ntakos, G.; Nielsen, J.F.; Svendsgaard, J.; Poulsen, R.; Christensen, S. Are Vegetation Indices Derived from Consumer-Grade Cameras Mounted on UAVs Sufficiently Reliable for Assessing Experimental Plots? *Eur. J. Agron.* **2016**, *74*, 75–92. [[CrossRef](#)]
24. Du, L.; Yang, H.; Song, X.; Wei, N.; Yu, C.; Wang, W.; Zhao, Y. Estimating Leaf Area Index of Maize Using UAV-Based Digital Imagery and Machine Learning Methods. *Sci. Rep.* **2022**, *12*, 15937. [[CrossRef](#)]
25. Siegmann, B.; Jarmer, T. Comparison of Different Regression Models and Validation Techniques for the Assessment of Wheat Leaf Area Index from Hyperspectral Data. *Int. J. Remote Sens.* **2015**, *36*, 4519–4534. [[CrossRef](#)]
26. Breiman, L. Random forests. *Mach. Learn.* **2001**, *45*, 5–32. [[CrossRef](#)]

27. Chemura, A.; Chemura, A.; Mutanga, O.; Dube, T. Separability of Coffee Leaf Rust Infection Levels with Machine Learning Methods at Sentinel-2 MSI Spectral Resolutions. *Precis. Agric.* **2017**, *18*, 859–881. [[CrossRef](#)]
28. Akbarian, S.; Rahimi Jamnani, M.; Xu, C.-Y.; Wang, W.; Lim, S. Plot Level Sugarcane Yield Estimation by Machine Learning on Multispectral Images: A Case Study of Bundaberg, Australia. *Inf. Process. Agric.* **2023**, *in press*. [[CrossRef](#)]
29. Borup, D.; Christensen, B.J.; Mühlbach, N.S.; Nielsen, M.S. Targeting predictors in random forest regression. *Int. J. Forecast.* **2023**, *39*, 841–868. [[CrossRef](#)]
30. Luo, P.; Liao, J.; Shen, G. Combining Spectral and Texture Features for Estimating Leaf Area Index and Biomass of Maize Using Sentinel-1/2, and Landsat-8 Data. *IEEE Access* **2020**, *8*, 53614–53626. [[CrossRef](#)]
31. Chen, Y.; Ma, L.; Yu, D.; Feng, K.; Wang, X.; Song, J. Improving Leaf Area Index Retrieval Using Multi-Sensor Images and Stacking Learning in Subtropical Forests of China. *Remote Sens.* **2022**, *14*, 148. [[CrossRef](#)]
32. Frost, T.; Lindon, J.C.; Tranter, G.E.; Koppenaal, D.W. Quantitative Analysis. In *Encyclopedia of Spectroscopy and Spectrometry*; Academic Press: Oxford, UK, 2017; pp. 811–815.
33. Roy, K.; Kar, S.; Das, R.N. Selected Statistical Methods in QSAR. In *Understanding the Basics of QSAR for Applications in Pharmaceutical Sciences and Risk Assessment*; Academic Press: Oxford, UK, 2015; pp. 191–229.
34. Verrelst, J.; Muñoz, J.; Alonso, L.; Delegido, J.; Rivera, J.P.; Camps-Valls, G.; Moreno, J. Machine Learning Regression Algorithms for Biophysical Parameter Retrieval: Opportunities for Sentinel-2 and -3. *Remote Sens. Environ.* **2012**, *118*, 127–139. [[CrossRef](#)]
35. Ji, S.; Gu, C.; Xi, X.; Zhang, Z.; Hong, Q.; Huo, Z.; Zhao, H.; Zhang, R.; Li, B.; Tan, C. Quantitative Monitoring of Leaf Area Index in Rice Based on Hyperspectral Feature Bands and Ridge Regression Algorithm. *Remote Sens.* **2022**, *14*, 2777. [[CrossRef](#)]
36. Kataoka, T.; Kaneko, T.; Okamoto, H.; Hata, S. Crop Growth Estimation System Using Machine Vision. In Proceedings of the 2003 IEEE/ASME International Conference on Advanced Intelligent Mechatronics (AIM 2003), Kobe, Japan, 20–24 July 2003. [[CrossRef](#)]
37. Montalvo, M.; Guerrero, J.M.; Romeo, J.; Emmi, L.; Guijarro, M.; Pajares, G. Automatic Expert System for Weeds/Crops Identification in Images from Maize Fields. *Expert Syst. Appl.* **2013**, *40*, 75–82. [[CrossRef](#)]
38. Woebbecke, D.M.; Meyer, G.; Von Bargen, K.; Mortensen, D.A. Shape Features for Identifying Young Weeds Using Image Analysis. *Trans. ASAE* **1995**, *38*, 271–281. [[CrossRef](#)]
39. Meyer, G.E.; Neto, J.C. Verification of Color Vegetation Indices for Automated Crop Imaging Applications. *Comput. Electron. Agric.* **2008**, *63*, 282–293. [[CrossRef](#)]
40. Louhaichi, M.; Borman, M.M.; Johnson, D.E. Spatially Located Platform and Aerial Photography for Documentation of Grazing Impacts on Wheat. *Geocarto Int.* **2001**, *16*, 65–70. [[CrossRef](#)]
41. Yang, Z.; Willis, P.; Mueller, R. Impact of Band-Ratio Enhanced Awifs Image to Crop Classification Accuracy. 2008. Available online: <http://www.asprs.org/a/publications/proceedings/pecora17/0041.pdf> (accessed on 25 January 2024).
42. Bendig, J.; Yu, K.; Aasen, H.; Bolten, A.; Bennertz, S.; Broscheit, J.; Gnyp, M.L.; Bareth, G. Combining UAV-Based Plant Height from Crop Surface Models, Visible, and near Infrared Vegetation Indices for Biomass Monitoring in Barley. *Int. J. Appl. Earth Obs. Geoinf.* **2015**, *39*, 79–87. [[CrossRef](#)]
43. Hunt, E.R.; Doraiswamy, P.C.; McMurtrey, J.E.; Daughtry, C.S.T.; Perry, E.M.; Akhmedov, B. A Visible Band Index for Remote Sensing Leaf Chlorophyll Content at the Canopy Scale. *Int. J. Appl. Earth Obs. Geoinf.* **2013**, *21*, 103–112. [[CrossRef](#)]
44. Gitelson, A.A.; Kaufman, Y.J.; Stark, R.; Rundquist, D. Novel Algorithms for Remote Estimation of Vegetation Fraction. *Remote Sens. Environ.* **2002**, *80*, 76–87. [[CrossRef](#)]
45. Hague, T.; Tillett, N.D.; Wheeler, H. Automated Crop and Weed Monitoring in Widely Spaced Cereals. *Precis. Agric.* **2006**, *7*, 21–32. [[CrossRef](#)]
46. Huete, A.R. Remote Sensing for Environmental Monitoring. *Environ. Monit. Charact.* **2004**, 183–206. [[CrossRef](#)]
47. Shao, G.; Han, W.; Zhang, H.; Liu, S.; Wang, Y.; Zhang, L.; Cui, X. Mapping Maize Crop Coefficient Kc Using Random Forest Algorithm Based on Leaf Area Index and UAV-Based Multispectral Vegetation Indices. *Agric. Water Manag.* **2021**, *252*, 106906. [[CrossRef](#)]
48. Qiao, L.; Gao, D.; Zhao, R.; Tang, W.; An, L.; Li, M.; Sun, H. Improving Estimation of LAI Dynamic by Fusion of Morphological and Vegetation Indices Based on UAV Imagery. *Comput. Electron. Agric.* **2022**, *192*, 106603. [[CrossRef](#)]
49. Smith, H.L.; McAusland, L.; Murchie, E.H. Don't Ignore the Green Light: Exploring Diverse Roles in Plant Processes. *J. Exp. Bot.* **2017**, *68*, 2099–2110. [[CrossRef](#)] [[PubMed](#)]
50. Zhang, Y.; Xu, Z.; Li, J.; Wang, R. Optimum Planting Density Improves Resource Use Efficiency and Yield Stability of Rainfed Maize in Semiarid Climate. *Front. Plant Sci.* **2021**, *12*, 752606. [[CrossRef](#)] [[PubMed](#)]
51. Brewer, K.; Clulow, A.; Sibanda, M.; Gokool, S.; Naiken, V.; Mabhaudhi, T. Predicting the Chlorophyll Content of Maize over Phenotyping as a Proxy for Crop Health in Smallholder Farming Systems. *Remote Sens.* **2022**, *14*, 518. [[CrossRef](#)]
52. Hasan, U.; Sawut, M.; Chen, S. Estimating the Leaf Area Index of Winter Wheat Based on Unmanned Aerial Vehicle RGB-Image Parameters. *Sustainability* **2019**, *11*, 6829. [[CrossRef](#)]
53. Ballesteros, R.; Moreno, M.; Barroso, F.; González-Gómez, L.; Ortega, J. Assessment of Maize Growth and Development with High- and Medium-Resolution Remote Sensing Products. *Agronomy* **2021**, *11*, 940. [[CrossRef](#)]
54. Marcial-Pablo, M.D.J.; Gonzalez-Sanchez, A.; Jimenez-Jimenez, S.I.; Ontiveros-Capurata, R.E.; Ojeda-Bustamante, W. Estimation of Vegetation Fraction Using RGB and Multispectral Images from UAV. *Int. J. Remote Sens.* **2018**, *40*, 420–438. [[CrossRef](#)]

55. Sanches, G.M.; Duft, D.G.; Kölln, O.T.; Cláudia, A.; Quassi, G.; Okuno, F.M.; Henrique, C.J.F. The Potential for RGB Images Obtained Using Unmanned Aerial Vehicle to Assess and Predict Yield in Sugarcane Fields. *Int. J. Remote Sens.* **2018**, *39*, 5402–5414. [[CrossRef](#)]
56. Chen, S.; Chen, Y.; Chen, J.; Zhang, Z.; Fu, Q.; Bian, J.; Cui, T.; Ma, Y. Retrieval of Cotton Plant Water Content by UAV-Based Vegetation Supply Water Index (VSWI). *Int. J. Remote Sens.* **2020**, *41*, 4389–4407. [[CrossRef](#)]
57. Gholinejad, S.; Fatemi, S.B. Optimum Indices for Vegetation Cover Change Detection in the Zayandeh-Rud River Basin: A Fusion Approach. *Int. J. Image Data Fusion* **2019**, *10*, 199–216. [[CrossRef](#)]
58. Liu, S.; Jin, X.; Nie, C.; Wang, S.; Yu, X.; Cheng, M.; Shao, M.; Wang, Z.; Tuohuti, N.; Bai, Y.; et al. Estimating Leaf Area Index Using Unmanned Aerial Vehicle Data: Shallow vs. Deep Machine Learning Algorithms. *Plant Physiol.* **2021**, *187*, 1551–1576. [[CrossRef](#)]
59. Chai, T.; Draxler, R.R. Root Mean Square Error (RMSE) or Mean Absolute Error (MAE)? *Geosci. Model Dev. Discuss.* **2014**, *7*, 1525–1534. [[CrossRef](#)]
60. Wolff, F.; Kolari, T.H.M.; Villoslada, M.; Tahvanainen, T.; Korpelainen, P.; Zamboni, P.A.P.; Kumpula, T. RGB Vs. Multispectral Imagery: Mapping Aapa Mire Plant Communities with Uavs. *Ecol. Indic.* **2023**, *148*, 110140. [[CrossRef](#)]
61. Furukawa, F.; Laneng, L.A.; Ando, H.; Yoshimura, N.; Kaneko, M.; Morimoto, J. Comparison of RGB and Multispectral Unmanned Aerial Vehicle for Monitoring Vegetation Coverage Changes on a Landslide Area. *Drones* **2021**, *5*, 97. [[CrossRef](#)]

Disclaimer/Publisher’s Note: The statements, opinions and data contained in all publications are solely those of the individual author(s) and contributor(s) and not of MDPI and/or the editor(s). MDPI and/or the editor(s) disclaim responsibility for any injury to people or property resulting from any ideas, methods, instructions or products referred to in the content.